

A Novel Hierarchical Light Field Coding Scheme Based on Hybrid Stacked Multiplicative Layers and Fourier Disparity Layers for Glasses-Free 3D Displays

Joshitha Ravishankar[†], Mansi Sharma^{†*}

Indian Institute of Technology Madras, Chennai 600036, India.

Abstract

This paper presents a novel hierarchical coding scheme for light fields based on transmittance patterns of low-rank multiplicative layers and Fourier disparity layers. The proposed scheme identifies multiplicative layers of light field view subsets optimized using a convolutional neural network for different scanning orders. Our approach exploits the hidden low-rank structure in the multiplicative layers obtained from the subsets of different scanning patterns. The spatial redundancies in the multiplicative layers can be efficiently removed by performing low-rank approximation at different ranks on the Krylov subspace. The intra-view and inter-view redundancies between approximated layers are further removed by HEVC encoding. Next, a Fourier disparity layer representation is constructed from the first subset of the approximated light field based on the chosen hierarchical order. Subsequent view subsets are synthesized by modeling the Fourier disparity layers that iteratively refine the representation with improved accuracy. The critical advantage of the proposed hybrid layered representation and coding scheme is that it utilizes not just spatial and temporal redundancies in light fields but efficiently exploits intrinsic similarities among neighboring sub-aperture images in both horizontal and vertical directions as specified by different predication orders. In addition, the scheme is flexible to

*Corresponding author

[†]These authors contributed equally to this work

Email addresses: ee19d401@smail.iitm.ac.in (Joshitha Ravishankar[†]), mansisharmaiitd@gmail.com, mansisharma@ee.iitm.ac.in (Mansi Sharma[†])

realize a range of multiple bitrates at the decoder within a single integrated system. The compression performance of the proposed scheme is analyzed on real light fields. We achieved substantial bitrate savings and maintained good light field reconstruction quality.

Keywords: Light field, Lossy compression, Layered 3D displays, Convolutional neural network, Krylov subspace, Low-rank approximation, Block Krylov singular value decomposition, Rate distortion optimization, Fourier transform, Fourier disparity layers

1. Introduction

The light field imaging and 3D display markets are growing rapidly. In recent years, we have seen autostereoscopic displays emerge as a potential alternative to stereoscopic 3D displays as it supports stereopsis and motion parallax from different viewing directions [1, 2, 3, 4]. Parallax-based and lenticular-based 3D display technology has still not reached up to the standards to simultaneously provide direction-dependent outputs without losing out on the resolution in reconstructing dense light fields. Emerging multi-layered light field displays provide continuous motion parallax, greater depth-of-field, and wider field-of-view, which are critical for reproducing realistic 3D vision. Tensor or multi-layered displays can accurately reproduce multi-view images or light fields simultaneously with high resolution using just a few light attenuating layers [5, 6, 7].

The typical structure of a multi-layered display is shown in Fig. 1. It consists of light-attenuating pixelized layers (*e.g.*, LCD panels) stacked in front of a backlight. On each layer, the transmittance of pixels can be controlled independently by carrying out multiplicative operations. Fig. 2 illustrates the light rays which pass through different combinations of pixels in stacked layers depending on the viewing directions. Efficient representation and coding of light rays in multi-layered 3D displays are essential for adaptation on different auto-stereoscopic platforms.

Existing light field coding approaches are based on raw lenslet image [8, 9,

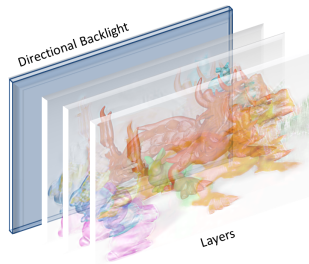


Figure 1: Structure of layered light field display

10, 11, 12], geometry information [13, 14, 15, 16], scene content information [17], disparity information [14, 13, 18], epipolar plane image-based and multiplane image-based [19, 15, 16], view prediction based learning schemes [20, 21, 22, 23] or methods considering light field data as a pseudo video sequence [24, 25, 26, 27]. These compression approaches are not specifically designed for tensor or multi-layered displays.

Our previous work on light field coding exploits the spatial and temporal correlations among light field multiplicative layers [28]. We handled the inherent redundancies in light fields by approximating multiplicative layers in the image-based spatial domain. In this work, we propose a novel hierarchical coding scheme for light field compression based on a hybrid multiplicative layers [29] and Fourier disparity layers representation [30]. The current approach efficiently deals with elimination of spatial, temporal and non-linear redundancies present in the light field view subsets while working in an integrated spatial and Fourier domain representation. This is a generalized coding scheme applicable to a variety of autostereoscopic displays, in particular, useful for tensor or multi-layer light field displays [1, 2, 3, 4]. It offers much more bitrate savings and adaptability to different coding approaches and also achieves the goal of covering a range of multiple bitrates in a single unified system. Apart from supporting multi-view and layered 3D displays, our model can complement other light field coding schemes based on learning networks to support various bitrates as well [31, 32, 33, 22, 34, 23].

In the proposed coding scheme, the input light field is divided into view sub-

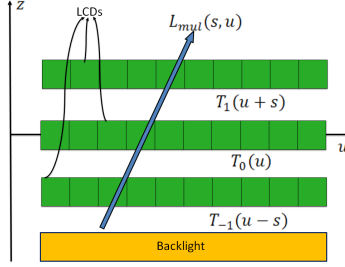


Figure 2: Configuration of multiplicative layers

sets based on pre-defined Circular and Hierarchical prediction orders (Fig. 3). Three optimized multiplicative layers for each view subset using convolutional neural networks (CNN) are constructed. The key idea in our proposed coding scheme is to reduce the dimensionality of stacked multiplicative layers using the randomized Block-Krylov singular value decomposition (BK-SVD) [35]. Factorization derived from BK-SVD effectively exploits the high spatial correlation between the multiplicative layers and approximates the light field subsets for varying low ranks. Encoding of these low-rank approximated subset multiplicative layers using HEVC codec [36] is performed to eliminate intra-view and inter-view redundancies further. Thus, our scheme approximates multiplicative layers of target light field view subsets for multiple ranks and quantization parameters (QPs) in the first stage. The view subsets are then reconstructed from the decoded layers.

In the second stage, the processing of the entire approximated light field is done in the Fourier domain, following a hierarchical coding procedure. A Fourier Disparity Layer (FDL) calibration is performed to estimate disparity values and angular coordinates of each light field view [37]. These essential parameters provide additional information for the FDL construction and view prediction. They are then transmitted to the decoder as metadata. Next, we split the approximated light field into subsets as identified by four scanning or prediction orders. The first set of views are encoded and utilized for constructing the FDL representation. This FDL representation synthesizes the succeeding view subsets.

The remaining correlations between the prediction residue of synthesized views and the approximated subset are further eliminated by encoding the residual signal using HEVC. The set of views obtained from decoding the residual are employed to refine the FDL representation and predict the next subset of views with improved accuracy. This hierarchical procedure continues iterating until all light field views are coded. The critical advantages of the proposed hybrid layered representation and coding scheme are:

- Our scheme efficiently exploits spatial, temporal, and non-linear redundancies between adjacent sub-aperture images in the light field structure within a single integrated framework. The scheme leverages the benefits of hybrid multiplicative layers and Fourier disparity layers representation in our hierarchical coding and prediction model for gaining superior compression efficiency without compromising reconstruction quality. In the first stage, we process light field in the spatial domain and remove the intra-view and inter-view redundancies among subset multiplicative layers. In the second stage, while working in the Fourier domain, our scheme ensures to eliminate the non-linear redundancies among adjacent views in both horizontal and vertical directions that exhibit high similarities. Experiments with various real light fields following different scanning orders demonstrate superior compression performance of our proposed model.
- The scheme is versatile to realize a range of multiple bitrates within a single integrated system trained using few convolutional neural networks. This characteristic of the proposed model complements existing light field coding systems or methods which usually support only specific bitrates during compression using multiple networks. Our coding model is adaptable to support various computational, multi-view auto-stereoscopic platforms, table-top, head-mounted displays, or mobile platforms by optimizing the bandwidth for a given target bitrate.

A shorter version of this work has been accepted for publication at IEEE SMC 2021 [38]. The current journal version is an extension that elaborates on

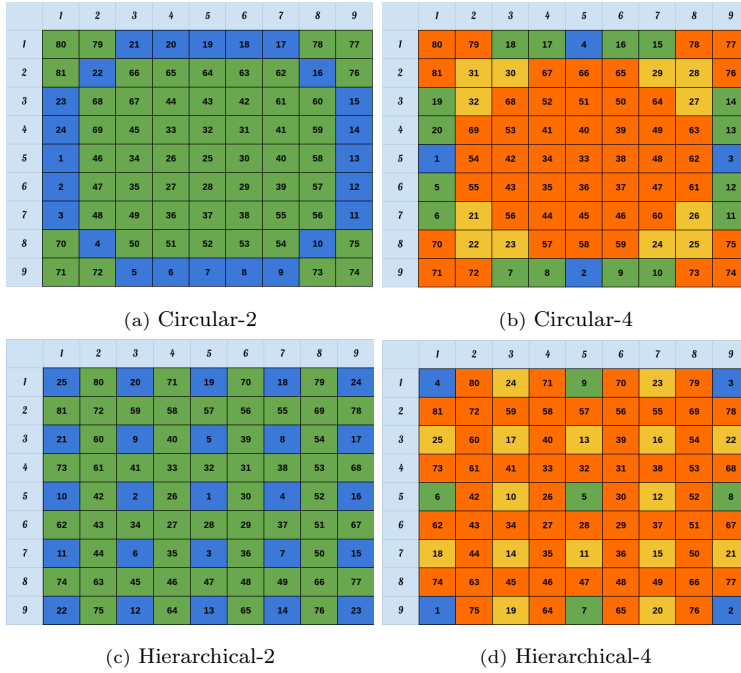


Figure 3: The light field view prediction orders C_2 , C_4 , H_2 & H_4 . Views in blue, green, yellow & orange form the first, second, third and fourth subset respectively.

two more light field scanning patterns for view subsets. It includes new detailed results and extensive analysis of the performance of the proposed light field coding model. The rest of this article is organized into four major sections. Section 2 describes various existing light field compression approaches and their shortcomings. The proposed layered representation and coding scheme for multi-view displays is discussed in Section 3 in detail. We have elaborated our experiments specifying the implementation, results, and analysis in Section 4. Lastly, the conclusion with comprehensive findings of our proposed scheme and implications of future work are presented in Section 5.

2. Related Works

The light field image or plenoptic image contains information about the intensity and direction of light rays in space [39, 40]. It involves a large volume

of data. Thus, the storage and transmission requirements for light fields are tremendous. Efficient compression techniques leveraging the data redundancy in both the spatial and angular domains of light fields are essential. Compression or coding techniques for light fields are often broadly classified into two categories; lenslet-based or approaches based on perspective sub-aperture images.

The direct compression using raw light field lenslet image captured by plenoptic camera exploits the spatial redundancy between the microimages [8, 9, 10, 11, 12]. This approach is usually based on the existing image/video coding standards, such as JPEG [41] or high efficiency video coding (HEVC) [42]. The unique light field structural characteristics make it harder to predict the lenslet image regions with complex textures accurately. Moreover, there are numerous microimages in the raw light field image which need careful handling. The microimages are of low resolution and require customized reshaping before being fed into an HEVC encoder. Ideally, the lenslet-based compression solutions need to transmit camera parameters for further processing, and thus increase the coding burden on the compressed data stream. These drawbacks encouraged researchers to extract the light field sub-aperture images (SAIs) from raw plenoptic images and explore compression possibilities on these views.

There are various coding methods that directly take light field SAIs as the input. They are broadly categorized as content-based compression [17], disparity-based [14, 13, 18], epipolar plane image-based and multiplane image-based [19, 15, 16], pseudo sequence based [24, 43, 25, 26, 27], view synthesis based [44, 45, 20, 21], and learning-based compression methods [31, 32, 33, 22, 34, 23].

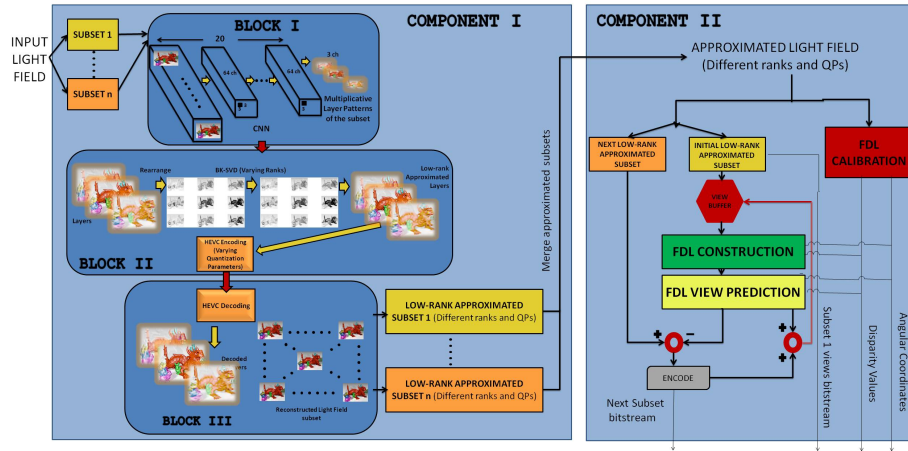
Disparity-based compression methods approximate particular views by the weighted sum of other views [14] or apply the homography-based low-rank approximation method called HLRA [13]. This approach depends on how much the disparities across views vary and may not optimally reduce the low-rank approximation error for light fields with large baselines. Dib et al. [18] proposed a novel parametric disparity estimation method to support the low-rank approximation using super rays. They efficiently exploit redundancy across the different views compared to the homography-based alignment. A shearlet

transform-based method presented in [15] categorizes the SAIs into key and decimated views. The scheme performs well under low bitrates. The decimated views are predicted from the compressed key views and a residual bitstream. Chen et al. [16] used multiplane representation and strongly reduced the calculation burden on the decoder.

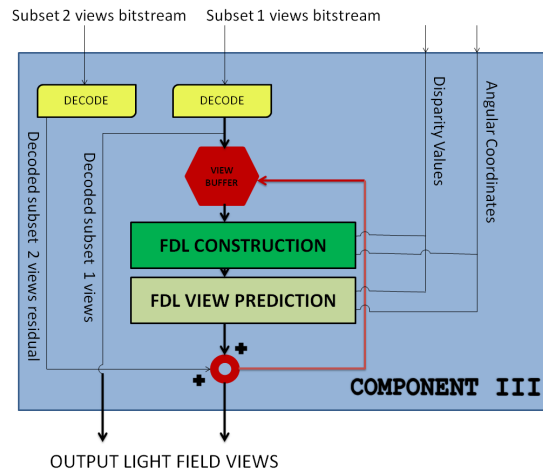
The views are reordered as pseudo sequences in predictive compression methods. Liu et al. [24] in their symmetric 2D hierarchical order, compresses the central view first as the I-frame (intra frame) followed by the remaining views as P-frames. Their prediction structure ensures inter-view prediction from adjacent views. Another proposal by Li et al. [43] involves dividing all the light field views into four quadrants and adopting a hierarchical coding structure within each quadrant. Ahmad et al. [25] utilize the multi-view extension of HEVC (MV-HEVC) to compress the light field in the form of a multi-view sequence. They interpret each row of the sub-aperture views as a single view of a multi-view video sequence and propose a two-dimensional prediction and rate allocation scheme. The extension of their work [26] uses hierarchical levels, where views belonging to higher levels are assigned with better quality. The higher-level views are used as references to predict the lower-level views. Synthesized virtual reference frames are generated from Adaptive Separable Convolution Network (ASCN) in another SAIs based technique [27]. Such frames are considered as extra reference candidates in a hierarchical coding structure for MV-HEVC to further exploit intrinsic similarities in light field images.

A block-basis estimation of views from translated reference views is proposed in [21]. The residuals of estimated views are also transmitted to the decoder along with the rest of the view estimation parameters. Other view synthesis compression schemes estimate image depth maps from a subset of reference light field views. The Multi-view Video plus Depth (MVD) structure is adopted for depth image-based rendering to synthesize the intermediate SAIs [45]. A pair of steps to generate noise-refined depth maps for selected perspective views is elaborated in [20].

Bakir et al. [31] presented a deep learning-based scheme on the decoder side



(a)



(b)

Figure 4: Three components of proposed light field coding scheme. (a) Overview of the encoding scheme (b) Overview of the decoding scheme.

to improve the reconstruction quality of sub-aperture images. Similarly, Zhao et al. [32] encoded only sparsely sampled SAIs, while the remaining SAIs are synthesized using a CNN from the decoded sampled SAIs as priors. However, these methods require large-scale and diverse training samples, and high quality of reconstructed views is only obtained if at least half the SAIs are taken as reference. Schioppa et al. [22] proposed a novel network that synthesizes the entire light field image as an array of synthesized macro pixels in one step. Wang et al. [33] identify a region of interest (ROI), a complex non-ROI, and a smooth non-ROI to compress light field videos frame-wise. A generative adversarial network (GAN) is proposed in [34] for unsampled SAIs generation. Liu et al. [23] also adopt a GAN framework to boost the light field compression. They use an image group-based sampling method to reduce more SAI redundancy and maintain the reconstructed SAI quality. A perceptual quality-based loss function is also proposed by considering the PSNR of synthetic SAIs and adversarial loss. The above-mentioned coding techniques are not explicitly designed for the representation used in multi-layer-based light field displays. They also usually train a system (or network) to support only specific bitrates during the compression.

3. Proposed Methodology

The complete workflow of our proposed representation and coding scheme with three main components is illustrated in Fig. 4. In COMPONENT I, input light field images are divided into view subsets depending on the specific prediction orders. To efficiently exploit the intrinsic redundancies in light field data, the proposed scheme constructs multiplicative layers from each view subset by employing a CNN. BLOCK I represents a CNN that converts the light field views of the input subsets into three multiplicative layers [29]. In BLOCK II, we removed the intrinsic redundancy present in subset views by exploiting the hidden low-rank structure of multiplicative layers on a Krylov subspace [35]. The low-rank approximation of each subset multiplicative layers is performed using Block-Krylov singular value decomposition (BK-SVD) by choosing various

ranks [35]. The intra-frame and inter-frame redundancies are further eliminated by encoding the approximated layers with HEVC [36]. We reconstruct the approximated views of each subset from their respective decoded multiplicative layers in BLOCK III. At the end of COMPONENT I of our scheme, we obtain approximated light field data at various ranks and quantization parameters.

In the next second phase, approximated subsets are used to construct Fourier disparity layer (FDL) representation of light fields [30]. The processing of approximated light field in COMPONENT II of our scheme is shown in Fig. 4a. There exist non-linear correlations between neighboring sub-aperture views in both horizontal and vertical directions in the light field structure. We particularly target these redundancies between adjacent light field views by processing in the Fourier domain as specified by different scanning or predication orders. The light field is then iteratively reconstructed by the FDL representation in a hierarchical fashion. We find the angular coordinates and disparity values of each view of the low-rank approximated light field (at different ranks and QPs) through FDL calibration and directly transmit them to the decoder (COMPONENT III) as metadata [37]. The approximated light field is divided into subsets specified by four different prediction orders. The initial subset is used in construction of the FDL representation, which is further employed to synthesize the subsequent subsets of views. The correlations in prediction residue are removed, and a more accurate FDL representation is constructed from previously encoded subsets. Thus, we iteratively refine the FDL representation in COMPONENT II until all the approximated light field views are encoded. The decoding scheme is depicted in COMPONENT III (Fig. 4b). Here, angular coordinates and disparity values of the low-rank approximated light field, along with the encoded bitstreams of approximated subsets are utilized for the final light field reconstruction.

3.1. Approximation of light field at different ranks

The input light field is divided into view subsets in COMPONENT I, depending on the specified scanning orders, and a low-rank approximated repre-

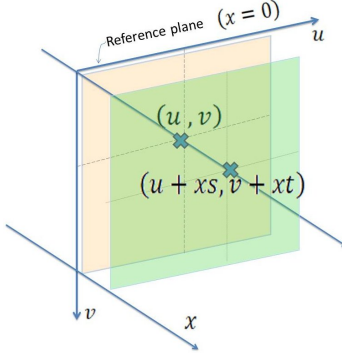


Figure 5: The light ray is parameterized by point of intersection with the (u, v) plane and the (s, t) plane located at a depth x .

sensation of the subset multiplicative layers is obtained in the Krylov subspace. BLOCK I to III in Fig. 4a illustrate the three sub-blocks involved in this step. The details of each step are described in the following sub-sections.

3.1.1. View Subsets of Light Field

The proposed scheme divides the light field into different view subsets based on predefined scanning orders. We adopt a hierarchical pattern configuration and a circular view prediction order described in the work of Dib et al. [37]. The four chosen patterns are Circular-2 (C_2), Circular-4 (C_4), Hierarchical-2 (H_2) and Hierarchical-4 (H_4). For a 9×9 light field, the C_2 and H_2 patterns contain two view subsets and C_4 and H_4 patterns have four subsets. The exact coding orders of each subset of these four chosen scanning orders are shown in Fig. 3. In all subsets of these patterns, the light field views form a circle that spiral out from the center. Generally, the corner views of light fields are of lower quality, and thus we choose to form a circle rather than a square while scanning the views. Our proposed workflow begins with partitioning of the input light field into subsets based on C_2 , C_4 , H_2 or H_4 patterns (Fig. 4).

3.1.2. Light Field Views to Stacked Multiplicative Layers

The light field $L(s, t, u, v)$ characterizes radiance along light rays as a 4D function [39, 40]. In $L(s, t, u, v)$, the parameters (s, t) specify the spatial coor-



Figure 6: The three optimal multiplicative layers produced by the CNN for the *Dragon and Bunnies* light field [46].

ordinates and (u, v) denote the angular coordinates that represent intersection of the rays with two parallel planes (Fig. 5). A light field can be interpreted as a set of directional views and can be produced using stacked layers that carry out multiplicative light ray operations [29]. Such multiplicative layers could be realized with few light-attenuating panels stacked in equally spaced intervals in front of a backlight (Fig. 1).

The normalized intensity of a light ray emitted from light field display can be described as

$$L_m(s, t, u, v) = \prod_{x \in X} T_x(u + xs, v + xt) \quad (1)$$

where, $T_x(u, v)$ is the transmittance of the layer present at disparity x and X denotes the set of disparities among directional views. We determined the multiplicative layers for each subset of different view scanning order. The experiments are performed by considering the light field display composed of three layers located at $X = \{-1, 0, 1\}$.

The three multiplicative layers obtained from each subset are optimized using a data-driven CNN based approach. The network architecture is depicted in Fig. 4a. The objective is to optimize the layer patterns. Mathematically, it is expressed as

$$\operatorname{argmin}_{T_x | x \in X} \sum_{s, t, u, v} \|L(s, t, u, v) - L_m(s, t, u, v)\|^2 \quad (2)$$

The optimized multiplicative layers obtained for 5×5 *Dragon and Bunnies* light field is shown in Fig. 6.

3.1.3. *Low-Rank Representation of Subset Multiplicative Layers on Krylov Subspace*

The randomized Block-Krylov SVD method introduced by Cameron and Christopher can optimally achieve the low-rank approximation of a matrix within $(1 + \epsilon)$ of optimal for spectral norm error [35]. The algorithm quickly converges in $\tilde{O}(\frac{1}{\sqrt{\epsilon}})$ iterations for any matrix. In our proposed scheme, the optimized multiplicative layers are compactly represented on a Krylov subspace in order to remove the intrinsic redundancy.

We denote each multiplicative layer pattern obtained from the CNN as $T_x \in \mathbb{R}^{m \times n \times 3}$, where $x \in \{-1, 0, 1\}$. The red, green, and blue colour channels of the layer x are denoted as T_x^r , T_x^g , and T_x^b respectively. We construct three matrices $A^{ch} \in \mathbb{R}^{3m \times n}$, $ch \in \{r, g, b\}$ as

$$A^{ch} = \begin{pmatrix} T_{-1}^{ch} \\ T_0^{ch} \\ T_1^{ch} \end{pmatrix} \quad (3)$$

The BK-SVD low-rank approximation in a Krylov subspace for each A^{ch} can remove the intrinsic redundancies in multiplicative layers of the subsets. For simplicity, we will denote A^{ch} as A henceforth. To approximate A , the objective is to achieve a subspace that closely captures the variance of A 's top singular vectors and avoid the gap dependence in singular values. The spectral norm low-rank approximation error of A is

$$\|A - DD^T A\|_2 \leq (1 + \epsilon) \|A - A_k\|_2 \quad (4)$$

Only top k singular vectors of A are used in its rank- k approximation A_k . If D is a rank- k matrix with orthonormal columns, the spectral norm guarantee ensures that $DD^T A$ recovers A up to a threshold ϵ .

Block Krylov iteration is performed working with the Krylov subspace

$$K = [\Pi \quad A\Pi \quad A^2\Pi \quad A^3\Pi \cdots A^q\Pi] \quad (5)$$

As analyzed in [35], we choose to work on low degree polynomials that allow faster computation in fewer powers of A , and thus enabling convergence of the

BK-SVD algorithm in fewer iterations. From subspace K , we construct $p_q(A)\Pi$ for any polynomial $p_q(\cdot)$ of degree q , where $\Pi \sim N(0, 1)^{d \times k}$. The approximation of A done by projecting it onto the span of $p_q(A)\Pi$ atleast matches the best k rank approximation of A lying in the span of Krylov space K [35]. Further, we orthonormalize columns of K to obtain $Q \in \mathbb{R}^{c \times qk}$ using QR decomposition method [47]. After computing SVD of matrix $S = Q^T B B^T Q$, we found matrix \bar{U}_k containing the top k singular vectors of S . Thus, the rank- k approximation of A is matrix D , which is computed as

$$D = Q\bar{U}_k \quad (6)$$

Consequently, the rank- k block Krylov approximation of matrices A^r , A^g and A^b are D^r , D^g , and D^b respectively. Matrix $D^{ch} \in \mathbb{R}^{y \times z}$ for every colour channel ch . To obtain the approximated layers \bar{T}_x , we extract colour channels from the approximated D^{ch} matrices by sectioning out the rows uniformly as

$$\begin{aligned} \bar{T}_{-1}^{ch} &= D^{ch}[1 : y, 1 : z] \\ \bar{T}_0^{ch} &= D^{ch}[y + 1 : 2y, 1 : z] \\ \bar{T}_1^{ch} &= D^{ch}[2y + 1 : 3y, 1 : z] \end{aligned}$$

The red, green, and blue colour channels are combined to form each approximated layer \bar{T}_{-1} , \bar{T}_0 , and \bar{T}_1 . Thus, factorization derived from BK-SVD exploits the spatial correlation in multiplicative layers of the subset views for varying low ranks. The three block Krylov approximated layers for each subset are subsequently encoded into a bitstream using HEVC for various QPs to further eliminate intra and inter layer redundancies in the low-rank approximated representation. The low-rank representation and coding of stacked multiplicative layers on Krylov subspace is depicted in BLOCK II of Fig. 4a.

3.1.4. Decoding and Reconstruction of the Light Field Subsets

The decoding procedure of compressed layers and the reconstruction of light field subsets is shown in BLOCK III of Fig. 4a. We decoded three multiplicative layers from the bitstream as \hat{T}_x , $x \in \{-1, 0, 1\}$. We consider the integers s^*, t^* ,

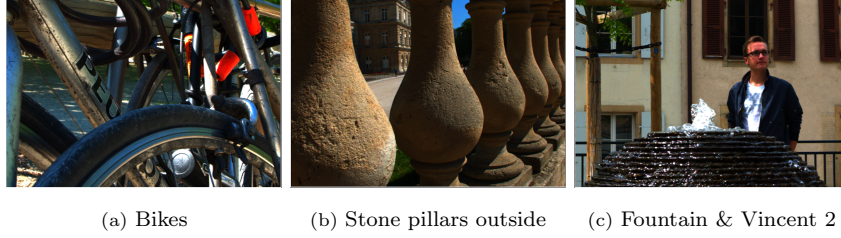


Figure 7: Central views of the three datasets.

which vary depending on the number of views in each subset. The view $I_{(s^*, t^*)}$ is obtained by translating the decoded layers to \hat{T}_x . This step is followed by an element-wise product of colour channels of the translated layers. For a particular view (s^*, t^*) , the translation of every x^{th} layer \hat{T}_x , to \hat{T}_x is carried out as

$$\hat{T}_{x(s^*, t^*)}(u, v) = \hat{T}_x(u + xs^*, v + xt^*) \quad (7)$$

Thus, the three translated layers for every viewpoint (s^*, t^*) is computed as

$$\begin{aligned} \hat{T}_{-1(s^*, t^*)}(u, v) &= \hat{T}_{-1}(u - s^*, v - t^*) \\ \hat{T}_{0(s^*, t^*)}(u, v) &= \hat{T}_0(u, v) \\ \hat{T}_{1(s^*, t^*)}(u, v) &= \hat{T}_1(u + s^*, v + t^*) \end{aligned}$$

An element-wise product of each colour channel $ch \in \{r, g, b\}$ of the translated layers give the corresponding colour channel of the subset view.

$$I_{(s^*, t^*)}^{ch} = \hat{M}_{-1(s^*, t^*)}^{ch} \odot \hat{M}_{0(s^*, t^*)}^{ch} \odot \hat{M}_{1(s^*, t^*)}^{ch} \quad (8)$$

The combined red, green and blue colour channels output the reconstructed light field subset at the viewpoint (s^*, t^*) as $I_{(s^*, t^*)}$. At last, we merged the view subsets according to C_2 , C_4 , H_2 or H_4 patterns.

Thus, the spatial correlation in multiplicative layers of the subset views is exploited for different low ranks in COMPONENT I of the proposed scheme. Intra and inter-layer redundancies in the low-rank approximated representation are also well removed. We further compressed the light field by eliminating intrinsic similarities caused by non-linear correlations among neighboring views

in horizontal and vertical directions as specified by C_2 , C_4 , H_2 and H_4 patterns using the Fourier Disparity Layers (FDL) representation. The following section describes the processing of approximated light fields in the Fourier domain.

3.2. Fourier Disparity Layers Representation & Light Field Processing

The Fourier Disparity Layers representation [30] samples the input BK-SVD approximated light field in the disparity dimension by decomposing it as a discrete sum of layers. The layers are constructed from the approximated light field sub-aperture views through a regularized least square regression performed independently at each spatial frequency in the Fourier domain. The FDL representation has been shown to be effective for numerous light field processing applications [30, 37, 48, 49]. We have summarised the use of FDL and encoding of low-rank approximated light field as COMPONENT II in Fig. 4a. The corresponding decoding and reconstruction of the light field subsets are illustrated as COMPONENT III in Fig. 4b. The Fourier Disparity Layer calibration, subset view synthesis, and prediction are described in the following subsections.

3.2.1. FDL Calibration

Without loss of generality, we have considered one spatial coordinate s and one angular coordinate u of 4D light field to present the notations in a simple manner. The approximated light field view L_{u_o} at angular position u_o can be defined as $L_{u_o}(s) = L(s, u_o)$. We can obtain Fourier coefficients of the j^{th} input light field view using n disparity values $\{d_k\}_{k \in [1, n]}$ [37]. The Fourier transform of L_{u_o} at spatial frequency f_s is

$$\hat{L}_{u_o}(f_s) = \sum_k e^{+2i\pi u_o d_k f_s} \hat{L}^k(f_s) \quad (9)$$

Here, the Fourier coefficients of the disparity layers for a particular frequency f_s is defined by

$$\hat{L}^k(f_s) = \int_{\Omega_k} e^{-2i\pi s f_s} L(s, 0) dx \quad (10)$$

Each of such Fourier coefficients can be understood as the Fourier transform of the central light field view (as $u_o = 0$ by just considering the spatial region Ω_k of disparity d_k).



(a) $C_2 - S1$ (b) $C_2 - S2$ (c) $C_4 - S1$ (d) $C_4 - S2$ (e) $C_4 - S3$ (f) $C_4 - S4$

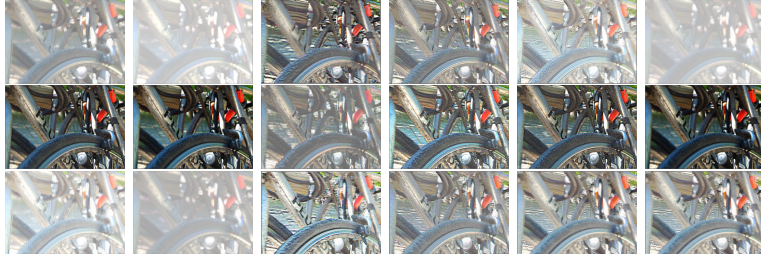
Figure 8: The multiplicative layers of each view subset (subset 1 to 4 denoted as S1 to S4) of the Circular-2 (C_2) and Circular-4 (C_4) scanning patterns. The first, second and third rows illustrate multiplicative layers -1, 0 and 1 respectively.

The angular coordinates u_j of the input views and the disparity values of the layers d_k are estimated by minimizing over all frequency components f_s^q , $q \in \llbracket 1, Q \rrbracket$, where Q is the number of pixels in each input image [30]. By computing Fourier transforms of all m approximated light field views as \hat{L}_{u_j} ($j \in \llbracket 1, m \rrbracket$), the FDL representation is learnt by solving a linear regression problem for each frequency f_s .

The optimization problem is formulated as $\mathbf{Ax} = \mathbf{b}$ with Tikhonov regularization, where $\mathbf{A} \in \mathbb{R}^{m \times n}$, $\mathbf{x} \in \mathbb{R}^{n \times 1}$ and $\mathbf{b} \in \mathbb{R}^{m \times 1}$. Elements of matrix \mathbf{A} are $\mathbf{A}_{jk} = e^{+2i\pi u_j d_k f_s}$ and \mathbf{x} contains the Fourier coefficients of disparity layers $\mathbf{x}_k = \hat{L}^k(f_s)$. The vector \mathbf{b} contains the Fourier coefficients of j^{th} input view, $\mathbf{b}_j = \hat{L}_{u_j}(f_s)$. The solution of the optimization problem results in the disparity values d_k and view positions u_j that are passed as metadata information to the decoder in COMPONENT III.

3.2.2. FDL View Synthesis and Prediction

In section 3.1.1, two basic scanning orders, circular and hierarchical, are discussed for the synthesis and coding of light field views. Each of these chosen orders has two or four view subsets. This results in four patterns C_2 , C_4 , H_2 and H_4 . In all four cases of the view prediction orders, the images are arranged in a spiral order starting from the center of the light field for each subset. The initial view subset of every pattern is always the first subset as specified by the



(a) $H_2 - S1$ (b) $H_2 - S2$ (c) $H_4 - S1$ (d) $H_4 - S2$ (e) $H_4 - S3$ (f) $H_4 - S4$

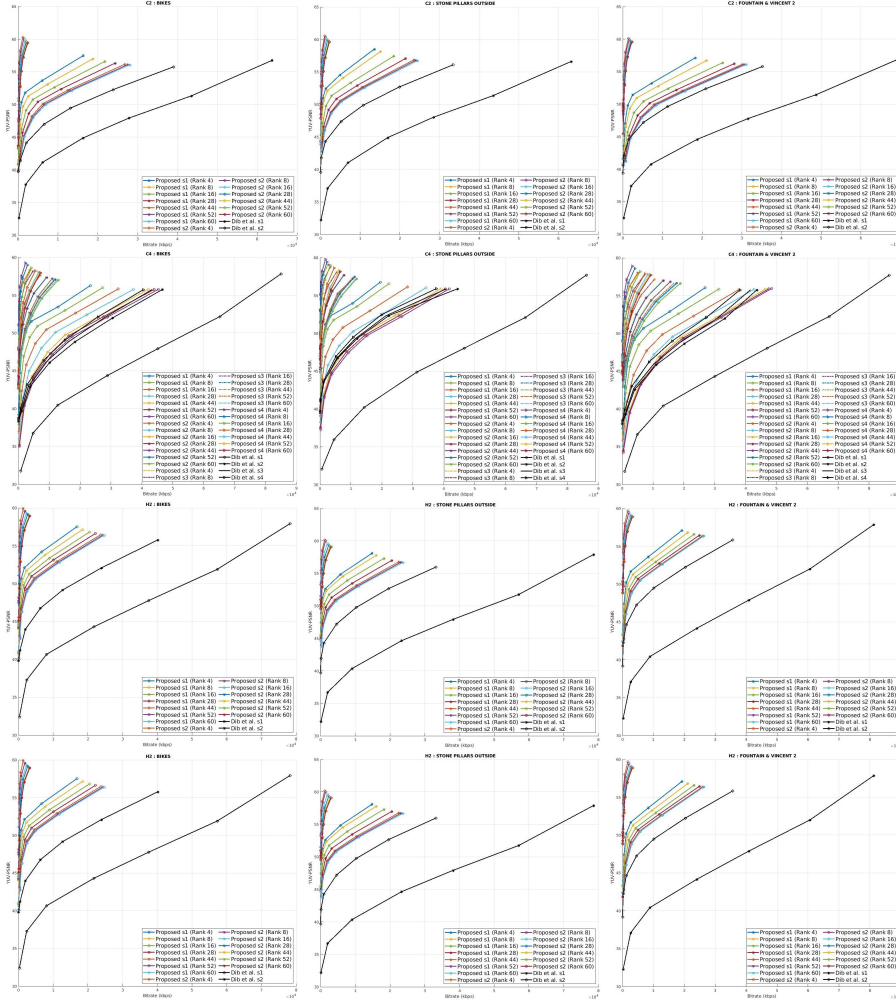
Figure 9: The multiplicative layers of each view subset (subset 1 to 4 denoted as S1 to S4) of the Hierarchical-2 (H_2) and Hierarchical-4 (H_4) scanning patterns. The first, second and third rows illustrate multiplicative layers -1, 0 and 1 respectively.

scanning order. This subset is directly encoded first in COMPONENT II. For example, in Fig. 3, the blue coloured subset in C_2 is the first subset.

The angular coordinates u_j and disparity values d_k are determined by the Fourier Disparity Layer calibration [30]. These are required in the further FDL construction and view predictions. This additional information is transmitted to the decoder in COMPONENT III as metadata [37]. The initial view subset is used in the basic construction of FDL representation. This aids in the synthesis of succeeding view subsets. The residual signal is also encoded to account for the remaining correlations in the prediction residue of synthesized views. The FDL representation is then refined before prediction and encoding of the next subset of views. Thus, the FDL representation is iteratively fine-tuned at every stage, after encoding every view subset, until all the approximated input light field views are encoded.

4. Results and Analysis

The performance of the proposed compression scheme is evaluated on real light fields captured by plenoptic cameras. The experiments are performed with *Bikes*, *Fountain & Vincent 2*, and *Stone pillars outside* light field datasets from the EPFL Lightfield JPEG Pleno database [50]. The central views of the chosen light field images are shown in Fig. 7. The raw plenoptic images are extracted



(a) Bikes (b) Stone pillars Outside (c) Fountain & Vincent 2

Figure 10: Bitrate vs YUV-PSNR curves for the proposed compression scheme and Dib et al. for the three datasets in the C_2 , C_4 , H_2 and H_4 patterns. (Kindly expand for better clarity)

into 15×15 sub-aperture views using the Matlab Light field toolbox [51].

The patterns C_2 , C_4 , H_2 and H_4 are constructed from inner 9×9 light field views for our experiments. Subsets 1 and 2 of C_2 contain 24 and 57 light field views respectively. The first and second subsets H_2 contain 25 and 56 views respectively. In C_4 , subsets 1, 2, 3 and 4 have 4, 16, 12 and 49 views respectively. Lastly, subsets 1, 2, 3 and 4 of H_4 contain 4, 5, 16 and 56 light field views respectively. The exact scanning orders of the patterns and their subsets are specified in Fig. 3.

4.1. Experimental Settings and Implementation Details

The proposed scheme is implemented on a single high-end HP OMEN X 15-DG0018TX system with 9th Gen i7-9750H, 16 GB RAM, RTX 2080 8 GB Graphics, and Windows 10 operating system. The multiplicative layers for each view subset of the four scanning orders are optimized using their corresponding convolutional neural network (CNN). The CNN contains twenty 2D convolutional layers stacked in a sequence. They have constant spatial size of tensors throughout and only the number of channels is varied. The first layer in each CNN corresponds to the tensor \mathbf{L} , which contains all the pixels of subset $L(u, v, s, t)$ being handled. \mathbf{L} has number of channels equal to the number of viewpoints in respective subset and tensor \mathbf{T} (that contained all the pixels of $T_x(u, v)$) has 3 channels corresponding to the 3 light field subset multiplicative layers. Intermediate convolutional layers comprise of 64 channels each. In Fig. 4a, ‘ch’ refers to the channels in the convolutional layers. We train each CNN model for 25 epochs at a learning rate of 0.001 and a batch size of 15. The entire networks are implemented using the Python-based framework, Chainer (version 7.7.0).

The resultant output multiplicative layers for each subset of C_2 , C_4 , H_2 and H_4 patterns are obtained from the trained CNN models. Fig. 8 illustrates the three multiplicative layers produced for each view subset of Circular-2 and Circular-4 patterns in the *Fountain & Vincent 2* data. The three multiplicative layers of each subset of Hierarchical-2 and Hierarchical-4 are shown in Fig. 9 for

Table 1: Total number of bytes for each subset of Circular-2 pattern using our proposed coding scheme and Dib et al. [37].

QP	Scheme	Bikes		Stone pillars outside		Fountain & Vincent 2	
		Subset 1	Subset 2	Subset 1	Subset 2	Subset 1	Subset 2
2	Dib et al.	6373276	9269248	6321523	7928095	6912472	8363327
	Proposed (Rank 4)	1634865	285016	1358448	243122	1827059	335430
	Proposed (Rank 8)	1877550	349216	1512085	283331	2115774	380847
	Proposed (Rank 16)	2177689	417606	1847285	351680	2519102	446949
	Proposed (Rank 28)	2438540	486569	2142502	418877	2806767	494263
	Proposed (Rank 44)	2674089	532163	2350849	487484	3008060	545947
	Proposed (Rank 52)	2749844	561758	2401859	503039	3063768	535674
	Proposed (Rank 60)	2805401	581882	2448047	527789	3113991	535619
6	Dib et al.	4350810	5663692	4354754	4732850	4869817	4963030
	Proposed (Rank 4)	602334	124074	493765	104272	728339	149454
	Proposed (Rank 8)	741293	165605	571942	130267	893240	178163
	Proposed (Rank 16)	916846	211107	761895	173837	1138839	220365
	Proposed (Rank 28)	1086119	247005	925727	218830	1349095	252514
	Proposed (Rank 44)	1252891	282873	1051703	256343	1499318	268165
	Proposed (Rank 52)	1311143	290011	1084796	268153	1547468	279455
	Proposed (Rank 60)	1354933	310371	1118995	281491	1583718	284981
10	Dib et al.	4350810	5663692	4354754	4732850	4869817	4963030
	Proposed (Rank 4)	602334	124074	493765	104272	728339	149454
	Proposed (Rank 8)	741293	165605	571942	130267	893240	178163
	Proposed (Rank 16)	916846	211107	761895	173837	1138839	220365
	Proposed (Rank 28)	1086119	247005	925727	218830	1349095	252514
	Proposed (Rank 44)	1252891	282873	1051703	256343	1499318	268165
	Proposed (Rank 52)	1311143	290011	1084796	268153	1547468	279455
	Proposed (Rank 60)	1354933	310371	1118995	281491	1583718	284981
14	Dib et al.	1635624	1555027	1697516	1227782	1879832	1231959
	Proposed (Rank 4)	85418	47842	60119	36583	124338	51127
	Proposed (Rank 8)	129326	64433	81540	45979	177036	66168
	Proposed (Rank 16)	197901	80959	136933	64691	279887	79125
	Proposed (Rank 28)	271565	98486	200957	79562	376807	94429
	Proposed (Rank 44)	347606	112747	255491	93448	449040	103222
	Proposed (Rank 52)	372263	119795	267999	97639	466826	103998
	Proposed (Rank 60)	389902	127835	280325	102454	483184	107398
20	Dib et al.	1635624	1555027	695581	292728	713369	335902
	Proposed (Rank 4)	85418	47842	25871	19602	54329	25826
	Proposed (Rank 8)	129326	64433	34316	23444	76408	33557
	Proposed (Rank 16)	197901	80959	55115	31584	116924	40566
	Proposed (Rank 28)	271565	98486	77665	38192	160911	47636
	Proposed (Rank 44)	347606	112747	99503	44221	187776	51037
	Proposed (Rank 52)	372263	119795	104642	46549	195728	52069
	Proposed (Rank 60)	389902	127835	109416	48116	203384	51973
26	Dib et al.	191049	125748	180485	36164	213553	66399
	Proposed (Rank 4)	18109	15295	12194	10550	26763	14884
	Proposed (Rank 8)	26471	20342	16372	13010	35126	18824
	Proposed (Rank 16)	36035	24566	22220	15525	46554	19651
	Proposed (Rank 28)	46328	28090	28818	17922	60959	23291
	Proposed (Rank 44)	55291	29746	35061	20507	70030	24332
	Proposed (Rank 52)	58525	30969	37056	20533	73670	24606
	Proposed (Rank 60)	61024	33335	39291	21200	75358	25193
38	Dib et al.	23065	7880	12613	1880	22582	2155
	Proposed (Rank 4)	2737	3283	2289	3043	5098	3887
	Proposed (Rank 8)	4208	4244	2719	3314	6606	4240
	Proposed (Rank 16)	5752	5095	3197	3572	7206	4708
	Proposed (Rank 28)	6864	5757	3888	3914	8261	4785
	Proposed (Rank 44)	7852	6246	4442	3969	9137	5104
	Proposed (Rank 52)	7946	6244	4437	4024	9294	5126
	Proposed (Rank 60)	8559	6592	4553	4038	9630	5197

Table 2: Total number of bytes for each subset of Hierarchical-2 pattern using our proposed coding scheme and Dib et al. [37].

QP	Scheme	Bikes		Stone pillars outside		Fountain & Vincent 2	
		Subset 1	Subset 2	Subset 1	Subset 2	Subset 1	Subset 2
2	Dib et al.	8149470	9362963	8187441	7746889	8467600	8311549
	Proposed (Rank 4)	1752364	327571	1544489	277441	2000768	399280
	Proposed (Rank 8)	1923491	425176	1668430	336414	2197190	475908
	Proposed (Rank 16)	2132305	534173	1904622	452160	2413070	576114
	Proposed (Rank 28)	2307124	626191	2137972	550384	2589097	663419
	Proposed (Rank 44)	2466765	728164	2348147	638116	2701529	709257
	Proposed (Rank 52)	2531862	732311	2415703	670368	2728626	732779
	Proposed (Rank 60)	2572006	759606	2470431	700779	2741756	740021
6	Dib et al.	5968201	5584732	5943824	4566311	6317422	4734277
	Proposed (Rank 4)	696307	141510	600337	110556	870560	169079
	Proposed (Rank 8)	796855	191515	665513	143058	991937	208585
	Proposed (Rank 16)	928516	259814	809014	209917	1119092	266975
	Proposed (Rank 28)	1044367	309978	953162	267569	1237456	314759
	Proposed (Rank 44)	1151050	364678	1079187	314645	1320242	341091
	Proposed (Rank 52)	1195073	376134	1122665	333719	1345621	355264
	Proposed (Rank 60)	1224508	388297	1153867	350318	1356529	359455
10	Dib et al.	3906437	2991907	3972408	2394424	4256777	2365804
	Proposed (Rank 4)	178206	74529	139283	54783	278393	83747
	Proposed (Rank 8)	234038	103767	176282	74433	350782	106751
	Proposed (Rank 16)	313521	143968	251942	112280	442029	138069
	Proposed (Rank 28)	389826	175682	336035	146248	523367	166752
	Proposed (Rank 44)	465603	213126	423251	172780	582988	184091
	Proposed (Rank 52)	493156	213184	449828	182623	600907	189758
	Proposed (Rank 60)	515966	221252	476680	192152	606755	192677
14	Dib et al.	2265550	1479998	2432694	1068158	2505792	1058776
	Proposed (Rank 4)	80756	43910	56613	32851	125237	48892
	Proposed (Rank 8)	108524	61888	74445	41825	162045	61496
	Proposed (Rank 16)	150025	85871	111220	63932	212590	78435
	Proposed (Rank 28)	191702	105961	151212	82963	264760	93719
	Proposed (Rank 44)	228876	121783	194620	96725	297942	104203
	Proposed (Rank 52)	243903	126699	209660	101918	309631	106855
	Proposed (Rank 60)	254844	129017	222970	106454	314274	109546
20	Dib et al.	842135	459805	946011	221956	926805	286174
	Proposed (Rank 4)	31602	20923	21663	15803	50142	23547
	Proposed (Rank 8)	43511	29373	28169	19788	63745	29074
	Proposed (Rank 16)	60423	40866	40732	28521	83392	35879
	Proposed (Rank 28)	76647	49200	53703	35594	103900	42129
	Proposed (Rank 44)	89653	56477	66649	41210	118608	45865
	Proposed (Rank 52)	94969	59779	71693	42630	121445	47138
	Proposed (Rank 60)	98186	61299	75923	44694	124309	47441
26	Dib et al.	242763	111266	213782	28940	272168	50062
	Proposed (Rank 4)	15705	11349	9646	7203	20645	11951
	Proposed (Rank 8)	20006	14619	12592	9004	27722	14167
	Proposed (Rank 16)	26014	19172	15947	12784	32178	15899
	Proposed (Rank 28)	30615	22252	19394	14768	39019	17819
	Proposed (Rank 44)	34692	25694	23190	16965	42684	19317
	Proposed (Rank 52)	36820	26082	25005	17802	44419	19885
	Proposed (Rank 60)	37464	26717	26359	18185	45207	19866
38	Dib et al.	26295	6202	13132	2001	22971	1975
	Proposed (Rank 4)	2485	2434	2065	2188	4019	3065
	Proposed (Rank 8)	3475	3205	2465	2484	4976	3523
	Proposed (Rank 16)	4143	3742	2736	2707	5456	3699
	Proposed (Rank 28)	4872	4364	3002	2868	6114	4137
	Proposed (Rank 44)	5280	4572	3121	2984	6327	4141
	Proposed (Rank 52)	5604	4810	3174	2980	6384	4192
	Proposed (Rank 60)	5704	4866	3205	3033	6467	4291

Table 3: Total number of bytes for each subset of Circular-4 pattern using our proposed coding scheme and Dib et al. [37].

QP	Scheme	Bikes				Stone pillars outside				Fountain & Vincent 2			
		Subset 1	Subset 2	Subset 3	Subset 4	Subset 1	Subset 2	Subset 3	Subset 4	Subset 1	Subset 2	Subset 3	Subset 4
2	Dib E et al.	1416866	3109571	5037933	12979009	1435611	2966575	4753968	12051303	1441765	2912377	4845501	12249516
	Proposed (Rank 4)	388099	258152	440152	768518	323881	173763	298852	569007	448166	341166	624766	1047411
	Proposed (Rank 8)	455053	324627	558934	968901	370490	225967	392536	740275	521873	472205	817319	1322771
	Proposed (Rank 16)	539142	479586	839084	1367088	472612	361397	632487	1084026	630974	695930	1211480	1864056
	Proposed (Rank 28)	620618	615680	1076100	1771137	570270	515012	906551	1475466	711522	887817	1536556	2377277
	Proposed (Rank 44)	701312	733863	1277639	2111200	651481	705884	1222296	1979756	773943	1039250	1785773	2679246
	Proposed (Rank 52)	732590	796888	1366241	2220068	675245	749842	1245301	1983765	792259	1177083	1968347	2854259
Proposed (Rank 60)	755916	864119	1454924	2314135	696777	789366	1336327	2114408	806779	1256248	2078412	2981898	
6	Dib E et al.	1086423	2038371	3237999	8276077	1106257	1486520	2490436	6394743	1117362	2219082	3574509	8740608
	Proposed (Rank 4)	214122	110706	188813	331799	175603	67554	116720	226090	256811	156184	289118	471852
	Proposed (Rank 8)	251850	151013	267156	453856	199275	93701	165247	308654	303608	234658	409134	641950
	Proposed (Rank 16)	309322	245463	439774	698158	269341	170374	302438	513257	385171	394167	678570	1001574
	Proposed (Rank 28)	370101	337259	595617	933555	341876	266334	474772	752003	454738	520966	898310	1310081
	Proposed (Rank 44)	434134	425824	737800	1151208	404438	384524	655959	1001388	507159	631820	1073918	1528251
	Proposed (Rank 52)	459408	462759	794905	1220896	425346	432563	711515	1073548	524083	727147	1192872	1641494
Proposed (Rank 60)	481777	511679	855678	1289391	440675	457735	766217	1149042	535587	785724	1271113	1730093	
10	Dib E et al.	752723	1222920	1913852	4856266	772216	801876	1330787	3442540	782679	1345211	2155105	5205636
	Proposed (Rank 4)	70222	49881	89829	166182	52813	29982	50755	103849	114218	79685	149995	246078
	Proposed (Rank 8)	103595	83335	144000	247091	73658	44585	77578	148404	152447	128770	220654	346457
	Proposed (Rank 16)	150921	135894	243209	385532	123883	87714	154861	265680	216590	228011	389982	561801
	Proposed (Rank 28)	200848	192706	340303	523869	178811	140370	254368	402085	271876	309157	522290	743004
	Proposed (Rank 44)	252927	249671	430367	652158	225984	223766	375786	553262	313974	379414	635701	880929
	Proposed (Rank 52)	272641	273179	463991	690749	241537	245429	399996	582554	327708	442106	715530	955029
Proposed (Rank 60)	289867	299732	497046	726508	253575	272199	437409	627469	336198	477148	795910	1002492	
14	Dib E et al.	480892	679589	1050351	2626996	521633	383952	638700	1648073	500828	742109	1187800	2801625
	Proposed (Rank 4)	40679	29652	51278	98485	29001	15388	25291	56627	65006	43589	81743	136374
	Proposed (Rank 8)	61694	44851	77249	140007	40184	23177	39845	80289	88848	66867	116614	189391
	Proposed (Rank 16)	91688	75524	135330	219789	69269	46427	79815	142707	131125	127103	212521	310005
	Proposed (Rank 28)	124841	108047	190712	296426	102889	75180	133133	214414	171095	175954	294598	419739
	Proposed (Rank 44)	158055	140028	240595	365750	133740	116563	195948	288671	198596	215928	358409	496160
	Proposed (Rank 52)	172129	153785	259051	385398	143679	127010	209194	303887	207304	252547	401949	532371
Proposed (Rank 60)	183237	167289	274776	401261	152195	136239	222340	319578	213372	275681	430690	564375	
20	Dib E et al.	213090	254203	381661	936738	237383	78987	150403	386715	220461	274582	434129	997828
	Proposed (Rank 4)	20074	11978	20998	45282	13422	5936	9649	25904	30830	17895	33796	60029
	Proposed (Rank 8)	29699	18356	30789	60782	18083	9076	14808	34361	41525	28044	48058	81843
	Proposed (Rank 16)	43104	29966	52919	92344	29269	17566	29273	57232	60581	47269	78364	121263
	Proposed (Rank 28)	58382	42027	73297	119860	42490	27054	49257	83411	79556	66517	110634	163393
	Proposed (Rank 44)	73197	53595	90516	142227	56027	39443	64624	100884	93770	81035	133102	188734
	Proposed (Rank 52)	78841	58178	96110	147314	60266	44362	71646	108650	98119	93685	147415	200453
Proposed (Rank 60)	83557	62421	100162	151331	63644	46378	73782	110035	100506	98744	154522	208763	
26	Dib E et al.	79458	76052	111845	267957	74881	8010	18414	52494	81501	76202	124228	276944
	Proposed (Rank 4)	9863	5121	8570	23184	6554	2967	4983	13967	15128	7839	15117	28897
	Proposed (Rank 8)	14088	8012	13369	33342	8505	4174	6644	17217	18704	11299	19552	35754
	Proposed (Rank 16)	19741	11666	19789	38861	12568	7266	12305	24932	25352	15455	26860	44990
	Proposed (Rank 28)	25182	15000	25496	46274	16190	9206	15165	29982	32582	21640	35738	57038
	Proposed (Rank 44)	30210	17987	29681	50997	20472	10873	19081	34787	37997	30815	46664	68833
	Proposed (Rank 52)	32119	19219	31116	52433	22260	11543	20113	36221	39422	27733	44203	65498
Proposed (Rank 60)	33288	19430	31422	52858	23179	11864	20961	37382	40662	28354	44886	66797	
38	Dib E et al.	13365	5614	8039	19199	9983	737	1149	2903	13141	3418	6028	13529
	Proposed (Rank 4)	2303	1128	1700	5087	1466	787	1257	3905	2733	1701	2922	6111
	Proposed (Rank 8)	3256	1399	2215	6353	1831	796	1249	3973	3418	1875	3098	6911
	Proposed (Rank 16)	4087	1792	2941	6919	2306	919	1475	4642	3888	2140	3599	7383
	Proposed (Rank 28)	5124	2025	3500	8088	2666	1017	1765	5011	4503	2291	4025	8008
	Proposed (Rank 44)	5542	2349	3864	8427	2949	1157	1992	5248	5240	2339	3980	7964
	Proposed (Rank 52)	5754	2458	3969	8508	3069	1177	2105	5587	5296	2432	4122	8436
Proposed (Rank 60)	5863	2536	4048	8389	3101	1149	1991	5345	5558	2435	4312	8577	

Table 4: Total number of bytes for each subset of Hierarchical-4 pattern using our proposed coding scheme and Dib et al. [37].

QP	Scheme	Bikes				Stone pillars outside				Fountain & Vincent 2			
		Subset 1	Subset 2	Subset 3	Subset 4	Subset 1	Subset 2	Subset 3	Subset 4	Subset 1	Subset 2	Subset 3	Subset 4
2	Dib E et al.	1440724	1452789	5165455	14131746	1441216	1362428	4475726	12790584	1491971	1430217	4898061	13465870
	Proposed (Rank 4)	369210	134008	323631	711432	319254	115673	265421	578809	427823	168575	540513	976300
	Proposed (Rank 8)	449987	189225	491920	944449	365506	138944	354594	733985	497979	236676	758310	1293087
	Proposed (Rank 16)	527356	284122	740612	1320068	461363	199211	550438	1042584	587856	308720	1036070	1653996
	Proposed (Rank 28)	594826	330343	938636	1687787	542214	264184	790867	1374410	669761	373958	1307700	2043902
	Proposed (Rank 44)	654269	396269	1161377	1988746	607986	334920	1018052	1718058	730933	513132	1660083	2511724
	Proposed (Rank 52)	675815	414816	1235023	2107314	632929	353228	1118538	1877849	757197	551166	1824076	2674922
Proposed (Rank 60)	696291	488035	1460949	2399511	650310	381130	1185575	1980309	776640	561102	1783246	2694231	
6	Dib E et al.	1111819	1038264	3514681	9168841	1108750	960856	2990048	8187927	1165584	1034953	3260693	8419196
	Proposed (Rank 4)	204317	62436	141660	311661	170346	51465	108216	241181	237931	96343	276107	473329
	Proposed (Rank 8)	245169	101036	243053	467936	197249	71588	166252	344009	283215	137939	410716	663983
	Proposed (Rank 16)	294934	153306	400324	701366	255205	110146	291160	544525	348866	195417	615257	934284
	Proposed (Rank 28)	344636	195036	539529	919037	314895	162077	451320	755049	410858	245260	809494	1190873
	Proposed (Rank 44)	395944	243143	691427	1120180	365865	208893	597212	959611	463453	324537	1030603	1465281
	Proposed (Rank 52)	415335	260202	745264	1191375	388987	224727	666304	1052010	488418	354981	1146980	1579657
Proposed (Rank 60)	431383	300783	885964	1357140	399568	236506	701288	1100371	504481	383573	1159853	1615488	
10	Dib E et al.	775655	666938	2142004	5440908	775397	625993	1827285	4832009	827917	670702	1897787	4726968
	Proposed (Rank 4)	62635	37584	75744	172831	50046	25982	50848	126123	100594	57683	146200	258515
	Proposed (Rank 8)	95314	60742	135199	271180	69850	35405	79321	176440	135538	85910	228956	369946
	Proposed (Rank 16)	137298	96352	230464	411368	113623	64943	154415	293640	185272	126344	364217	548547
	Proposed (Rank 28)	179852	124355	318267	535924	160773	100419	257622	431745	235083	160710	494057	711798
	Proposed (Rank 44)	222286	157319	416397	663668	199480	129589	348407	554301	277377	207598	626034	870952
	Proposed (Rank 52)	237984	167861	448807	703844	213343	143137	394288	609943	293737	229906	711584	949928
Proposed (Rank 60)	252828	190614	532675	790999	224197	145857	405564	625081	305891	247286	714102	964923	
14	Dib E et al.	500049	388083	1191431	2963845	513183	378425	1007183	2594115	541926	378184	988038	2383130
	Proposed (Rank 4)	37151	21951	41475	104839	28674	16217	30015	74285	56057	35279	82651	149587
	Proposed (Rank 8)	57510	37209	75972	161312	39181	21571	43882	103726	78222	52274	125153	213294
	Proposed (Rank 16)	84762	59234	128341	243684	63968	37448	83762	167620	110915	78720	204995	319141
	Proposed (Rank 28)	112659	77934	182347	317020	91763	55481	130123	240029	144823	100782	282460	414813
	Proposed (Rank 44)	139924	97313	239016	389102	116872	76489	191692	313499	171103	121884	353503	497967
	Proposed (Rank 52)	150018	104436	256212	409471	126814	82765	212476	335104	181934	144534	412929	555576
Proposed (Rank 60)	159098	115299	305078	457263	132712	88355	222964	347488	190145	145263	397671	546693	
20	Dib E et al.	220871	155877	442338	1069809	221668	144280	323891	808099	240428	132454	317605	742520
	Proposed (Rank 4)	18693	9386	16817	49155	14681	6261	12388	38873	27684	17171	34590	69842
	Proposed (Rank 8)	28822	17725	32732	79384	18981	10397	19570	51678	37767	23972	50490	96406
	Proposed (Rank 16)	42123	27257	52383	112254	29375	17001	34307	76671	53174	35808	79916	136134
	Proposed (Rank 28)	54836	35292	71902	136347	40267	21487	45165	93643	69187	45105	111945	176694
	Proposed (Rank 44)	66687	42676	92133	161840	51066	29424	66927	119603	80368	54863	136769	200474
	Proposed (Rank 52)	71351	45196	97830	166948	55199	30240	71069	121892	83943	59049	146132	205276
Proposed (Rank 60)	74991	47735	114919	183393	58046	33606	77786	128307	86632	61772	151950	212506	
26	Dib E et al.	80816	51560	127832	306862	70635	35903	66479	163981	88935	34759	71299	167645
	Proposed (Rank 4)	9615	3901	7759	27704	7357	2136	4879	18330	13811	7502	13052	31445
	Proposed (Rank 8)	14339	7033	13249	40246	9352	3875	7448	22526	17877	9379	19699	43266
	Proposed (Rank 16)	19865	10767	19976	53272	13320	5723	10509	30017	23372	12724	25181	52259
	Proposed (Rank 28)	25090	13451	25385	58593	16450	6534	14970	35654	29631	15747	34124	63501
	Proposed (Rank 44)	29298	15253	30770	63818	19658	8361	16303	40251	33967	17384	37712	67354
	Proposed (Rank 52)	30893	15025	29329	62347	20976	9012	19664	41450	35155	18862	42001	67561
Proposed (Rank 60)	31911	15795	32651	66267	22010	9312	20796	42488	35670	19892	43887	69423	
38	Dib E et al.	12808	5091	10029	22576	9452	2567	3519	6282	13878	1650	2798	5890
	Proposed (Rank 4)	2070	697	1396	5099	1470	511	1120	4115	3161	1300	2589	7469
	Proposed (Rank 8)	3312	1179	2248	7874	1817	604	1350	5095	3839	1278	2615	7893
	Proposed (Rank 16)	4414	1452	2788	9105	2418	768	1562	5528	4534	1754	3159	8763
	Proposed (Rank 28)	5149	1711	3140	9691	2826	777	1460	6012	5114	1616	3265	9168
	Proposed (Rank 44)	5836	1842	3717	11701	3085	1173	2064	6325	5833	2084	4167	10721
	Proposed (Rank 52)	6056	2071	3957	11951	3333	1056	1998	6683	5905	1891	4093	10013
Proposed (Rank 60)	6124	1844	3440	10214	3445	1113	2127	6741	5953	1987	3931	10061	

Table 5: Bjontegaard percentage rate savings for the proposed compression scheme with respect to Dib et al. [37]. Negative values represent gains.

Scene	Rank	Circular-2		Hierarchical-2		Circular-4				Hierarchical-4			
		Subset 1	Subset 2	Subset 1	Subset 2	Subset 1	Subset 2	Subset 3	Subset 4	Subset 1	Subset 2	Subset 3	Subset 4
Bikes	4	-97.56541214	-99.29882593	-98.3907291	-99.54258115	-96.20857709	-99.34681784	-99.32842039	-99.34121406	-96.7351185	-99.00868427	-99.47500508	-99.34379191
	8	-95.76892379	-99.03123267	-97.66246664	-99.29956835	-93.72289918	-98.65123258	-98.60472387	-98.82635815	-94.28513258	-97.74418081	-98.647811	-98.71977919
	16	-93.17474979	-98.45339444	-96.63095962	-98.95497164	-89.76525824	-97.16858635	-96.92654865	-98.03975782	-90.71898512	-95.38280704	-97.04688734	-97.88951207
	28	-90.3477664	-98.11361299	-95.58497187	-98.67266268	-84.94581006	-95.34857594	-94.83394299	-97.03298825	-86.86256935	-92.89572507	-95.15379369	-97.0052932
	44	-87.34955344	-97.75859383	-94.60404741	-98.07437089	-79.85797265	-92.77852898	-92.20674636	-95.85782231	-82.89202874	-90.05487069	-92.67313576	-96.06675045
	52	-86.18089698	-97.59830221	-94.16664723	-97.93405439	-77.60680642	-91.69706112	-91.16454361	-95.4561184	-81.31504874	-89.00949178	-91.89758467	-95.79899808
60	-85.37903466	-97.4382535	-93.89176465	-97.88383496	-75.79473857	-90.6698963	-90.38054322	-95.1466604	-80.07701534	-87.21412008	-90.0680445	-95.07426992	
Stone pillars outside	4	-98.28738998	-99.5671618	-98.54643236	-99.69494577	-96.70390985	-99.63514874	-99.63502461	-99.59656973	-96.57281486	-99.34377591	-99.50760509	-99.37042389
	8	-97.48146218	-99.45696678	-97.88804729	-99.65675017	-96.83115691	-99.35667758	-99.32191491	-99.35202452	-96.76795633	-99.10596584	-98.99132784	-99.12125107
	16	-95.3611157	-98.79333481	-96.93436888	-99.10493755	-93.99292616	-98.16597465	-98.2962672	-98.53366947	-94.36508582	-98.03801948	-98.47550354	-98.3838342
	28	-93.25557142	-98.75966092	-95.85758052	-98.75257079	-90.4631812	-96.53677355	-96.49717131	-97.50938121	-91.45018488	-97.04731002	-97.62269234	-98.45732096
	44	-91.33970709	-98.53538189	-94.86352824	-98.5749095	-86.68637432	-93.88697432	-94.29482711	-97.03694131	-88.48088951	-95.14677527	-95.98370386	-97.95248612
	52	-91.07697181	-98.45815322	-94.57758068	-98.46705075	-85.22044971	-93.13489515	-93.67714426	-96.75798999	-87.20785431	-94.70593446	-95.65455146	-97.72227925
60	-90.76161372	-98.35636369	-94.30087553	-98.40819422	-84.15256024	-93.01769387	-93.33095286	-96.66548892	-86.25854702	-94.27613508	-95.06018928	-97.5857605	
Fountain & Vincent 2	4	-96.27656828	-99.26603902	-96.9530291	-99.57099646	-93.24324684	-98.55291445	-98.36932301	-98.98906935	-94.92713556	-97.50272257	-98.13359141	-98.93827929
	8	-94.48002919	-98.96179277	-96.34841383	-99.08720888	-90.2813932	-97.37199047	-97.20967603	-98.62957034	-92.52170343	-95.77161689	-96.4265349	-98.44379923
	16	-91.14745649	-99.02010069	-95.17447177	-99.23270338	-84.41060243	-94.13934209	-93.80215798	-97.62140921	-88.53676951	-92.8003062	-94.58597524	-97.81833936
	28	-87.71507969	-98.92810522	-93.90335982	-98.97503776	-78.21793701	-92.83126167	-91.91796171	-96.58176205	-83.95868385	-91.25156494	-92.28424221	-96.94553427
	44	-85.20018338	-98.74257926	-92.71888896	-98.94441882	-73.07216196	-91.43574166	-90.58850443	-95.97145607	-80.11693215	-86.79417239	-88.96051247	-95.75589133
	52	-84.44629524	-98.77812886	-92.50450918	-98.83289017	-71.5870472	-89.37972401	-88.61773338	-95.48946614	-78.80228046	-85.31225663	-87.39959326	-95.3181428
60	-83.73495541	-98.74446465	-92.34241435	-98.90331735	-70.27253249	-88.33184967	-87.93389356	-95.17732486	-77.72435271	-85.15958083	-87.64733413	-95.43459988	

the *Bikes* data. We rearranged the colour channels of these multiplicative layers as described in section 3.1.3 and then applied BK-SVD for ranks 4, 8, 16, 28, 44, 52 and 60. The approximated matrices are then arranged back into layers and compressed using HEVC (BLOCK II of COMPONENT I). We use quantization parameters 2, 6, 10, 14, 20, 26, and 38 to test both high and low bitrate cases of HEVC. The decoding and reconstruction of BK-SVD approximated subsets for all four patterns are then performed.

Low-rank approximated subsets are then utilized to form the FDL representation of light fields. The number of layers in the FDL method are fixed to $n = 30$. Views in approximated Subset 1 construct the initial FDL representation. The subsequent view subsets are predicted from this FDL representation and the residues iteratively refine the FDL representation. We used HEVC to perform the encoding in COMPONENT II, choosing quantization parameters 2, 6, 10, 14, 20, 26 and 38. The final reconstructed light field central views at the end of COMPONENT III for the *Stone pillars outside* data is illustrated in Fig. 11 for the BK-SVD ranks 28, 44 and 60.

4.2. Results and Comparative Analysis

We compare the proposed scheme with Dib et al. [37] light field coding algorithm. The proposed coding scheme outperforms by large margins. The total number of bytes taken by our approach is comparatively far lesser than the work by Dib et al. [37] for all ranks and QPs. The corresponding results are depicted in Table 1 for C_2 , Table 2 for H_2 , Table 3 for C_4 and Table 4 for H_4 patterns. The bitrate vs YUV-PSNR graphs of three datasets in C_2 , C_4 , H_2 and H_4 configurations are illustrated in Fig. 10. For all four scanning patterns, the proposed scheme has significantly better rate-distortion results considering both subset-wise light field and entire light field.

Further, we analyze bitrate reduction (BD-rate) of the proposed scheme with respect to Dib et al. [37] using Bjontgaard metric [52]. The average percent difference in rate change is estimated over a range of QPs for seven chosen ranks. A comparison of the percentage of bitrate savings of our proposed coding scheme with respect to the anchor method for three chosen light field datasets is shown in Table 5. For C_2 pattern, the proposed scheme achieves 94.53%, 96.39%, and 93.96% bitrate reduction compared to Dib et al. [37] for light fields *Bikes*, *Stone pillars outside*, and *Fountain & Vincent 2* respectively. For pattern H_2 , the proposed scheme achieves 97.23%, 97.54%, and 96.67% bitrate reduction compared to Dib et al. [37] for the light fields *Bikes*, *Stone pillars outside*, and *Fountain & Vincent 2* respectively. Lastly, the C_4 and H_4 patterns have 93.09%, 95.29%, 90.71%, and 93.18%, 96.02%, 91.25% bitrate reduction respectively in the proposed scheme over Dib et al. [37] for *Bikes*, *Stone pillars outside*, and *Fountain & Vincent 2*.

5. Conclusion

We have proposed a novel hierarchical hybrid coding scheme for light fields based on transmittance patterns of low-rank multiplicative layers and Fourier Disparity Layers. Typical pseudo sequence based light field compression schemes [24, 25, 26, 27] do not efficiently consider the similarities between horizontal and

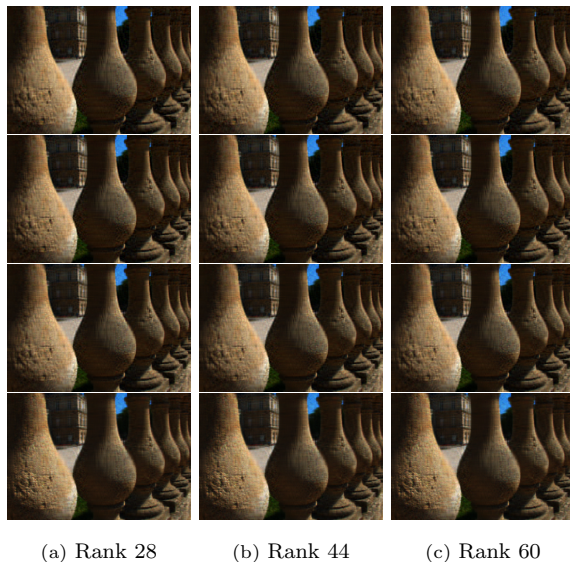


Figure 11: The central views of the reconstructed *Stone pillars outside* data for ranks 28, 44 and 60, encoded with a quantization of 2. The The first, second, third and fourth rows show results of Circular-2, Circular-4, Hierarchical-2 and Hierarchical-4 respectively.

vertical views of a light field. Our proposed scheme not only exploits the spatial correlation in multiplicative layers of the subset views for varying low ranks, but also removes the temporal intra and inter-layer redundancies in the low-rank approximated representation of view subsets. The approximated light field is further compressed by eliminating intrinsic similarities among neighboring views of Circular-2, Circular-4, Hierarchical-2 and Hierarchical-4 patterns using Fourier Disparity Layers representation. This integrated compression achieves excellent bitrate reductions without compromising the quality of the reconstructed light field.

Our scheme offers flexibility to cover a range of multiple bitrates using just a few trained CNNs to obtain a layered representation of the light field subsets. This critical feature sets our proposed scheme apart from other existing light field coding methods, which usually train a system (or network) to support only specific bitrates during the compression. Besides, existing coding approaches are not explicitly designed to target layered displays and are usually only classified

to work for lenslet-based formats or sub-aperture images based pseudo-sequence light field representation. The proposed flexible coding scheme can support not just multi-layered light field displays, but is also adaptable to table-top [53] or other variety of autostereoscopic displays.

In our future work, we plan to extend the proposed idea to light field displays with more than three light attenuating layers. Proof-of-concept experiments with our scheme also pave the way to form a more profound understanding in the rank-analysis of a light-field using other mathematically valid tensor-based models [6, 54] and coded mask cameras [55]. We also aim to verify our scheme with physical light field display hardware. Further, we wish to adapt the proposed scheme with display device availability and optimize the bandwidth for a target bitrate. This would enable deploying the concepts of layered displays on different display platforms that deliver 3D contents with limited hardware resources and thus best meet the viewers' preferences for depth impression and visual comfort.

Author contributions

Joshitha Ravishankar: Methodology, Software, Validation, Formal analysis, Investigation, Data Curation, Writing- Original Draft, Visualization. **Mansi Sharma:** Conceptualization, Methodology, Software, Validation, Formal analysis, Investigation, Resources, Writing- Original Draft, Supervision, Project administration.

Acknowledgement

The scientific efforts leading to the results reported in this paper have been carried out under the supervision of Dr. Mansi Sharma, INSPIRE Hosted Faculty, IIT Madras. This work has been supported, in part, by the Department of Science and Technology, Government of India project “*Tools and Processes for Multi-view 3D Display Technologies*”, DST/INSPIRE/04/2017/001853.

We would like to thank Nikitha Varma Sunchu and P Sai Shankar Pavan Srinivas for their help in running the codes for experiments.

Declaration of interests

The authors declare that they have no known competing financial interests or personal relationships that could have appeared to influence the work reported in this paper.

References

- [1] P. Surman, X. W. Sun, Towards the reality of 3d imaging and display, in: 2014 3DTV-Conference: The True Vision-Capture, Transmission and Display of 3D Video (3DTV-CON), IEEE, 2014, pp. 1–4.
- [2] T. Balogh, P. T. Kovács, A. Barsi, Holovizio 3d display system, in: 2007 3DTV Conference, IEEE, 2007, pp. 1–4.
- [3] Y. Kubota, N. Umezu, Pseudo-3d display based on head tracking for view-point image generation, in: 2019 IEEE 8th Global Conference on Consumer Electronics (GCCE), 2019, pp. 158–161. doi:10.1109/GCCE46687.2019.9015351.
- [4] P. Surman, X. Zhang, W. Song, X. Xia, S. Wang, Y. Zheng, Glasses-free 3-d and augmented reality display advances: From theory to implementation, *IEEE MultiMedia* 27 (1) (2020) 17–26. doi:10.1109/MMUL.2019.2948334.
- [5] T. Li, Q. Huang, S. Alfaro, A. Supikov, J. Ratchiff, G. Grover, R. Azuma, Light-field displays: a view-dependent approach, in: *ACM SIGGRAPH 2020 ET*, 2020, pp. 1–2.
- [6] G. Wetzstein, D. R. Lanman, M. W. Hirsch, R. Raskar, Tensor displays: compressive light field synthesis using multilayer displays with directional backlighting.

- [7] M. Sharma, S. Chaudhury, B. Lall, A novel hybrid kinect-variety-based high-quality multiview rendering scheme for glass-free 3d displays, *IEEE TCSVT* 27 (10) (2016) 2098–2117.
- [8] Y. Li, M. Sjöström, R. Olsson, U. Jennehag, Efficient intra prediction scheme for light field image compression, in: 2014 IEEE International conference on acoustics, speech and signal processing (ICASSP), IEEE, 2014, pp. 539–543.
- [9] C. Perra, P. Assuncao, High efficiency coding of light field images based on tiling and pseudo-temporal data arrangement, in: 2016 IEEE International Conference on Multimedia & Expo Workshops (ICMEW), IEEE, 2016, pp. 1–4.
- [10] Y. Li, R. Olsson, M. Sjöström, Compression of unfocused plenoptic images using a displacement intra prediction, in: 2016 IEEE ICMEW, IEEE, 2016, pp. 1–4.
- [11] R. J. Monteiro, P. J. Nunes, N. M. Rodrigues, S. M. Faria, Light field image coding using high-order intrablock prediction, *IEEE JSTSP* 11 (7) (2017) 1120–1131.
- [12] D. Liu, P. An, R. Ma, W. Zhan, X. Huang, A. A. Yahya, Content-based light field image compression method with gaussian process regression, *IEEE TM* 22 (4) (2019) 846–859.
- [13] X. Jiang, M. Le Pendu, R. A. Farrugia, C. Guillemot, Light field compression with homography-based low-rank approximation, *IEEE JSTSP* 11 (7) (2017) 1132–1145.
- [14] S. Zhao, Z. Chen, Light field image coding via linear approximation prior, in: *IEEE ICIP*, IEEE, 2017, pp. 4562–4566.
- [15] W. Ahmad, S. Vagharshakyan, M. Sjöström, A. Gotchev, R. Bregovic, R. Olsson, Shearlet transform-based light field compression under low bitrates, *IEEE TIP* 29 (2020) 4269–4280.

- [16] Y. Chen, P. An, X. Huang, C. Yang, D. Liu, Q. Wu, Light field compression using global multiplane representation and two-step prediction, *IEEE SPL* 27 (2020) 1135–1139.
- [17] X. Hu, J. Shan, Y. Liu, L. Zhang, S. Shirmohammadi, An adaptive two-layer light field compression scheme using gnn-based reconstruction, *ACM TOMM* 16 (2s) (2020) 1–23.
- [18] E. Dib, M. Le Pendu, X. Jiang, C. Guillemot, Local low rank approximation with a parametric disparity model for light field compression, *IEEE TIP* 29 (2020) 9641–9653.
- [19] S. Vagharshakyan, R. Bregovic, A. Gotchev, Light field reconstruction using shearlet transform, *IEEE transactions on pattern analysis and machine intelligence* 40 (1) (2017) 133–147.
- [20] X. Huang, P. An, F. Cao, D. Liu, Q. Wu, Light-field compression using a pair of steps and depth estimation, *Optics express* 27 (3) (2019) 3557–3573.
- [21] B. Hériard-Dubreuil, I. Viola, T. Ebrahimi, Light field compression using translation-assisted view estimation, in: *2019 PCS, IEEE*, 2019, pp. 1–5.
- [22] I. Schiopu, A. Munteanu, Deep-learning-based macro-pixel synthesis and lossless coding of light field images, *APSIPA TSIP* 8.
- [23] D. Liu, X. Huang, W. Zhan, L. Ai, X. Zheng, S. Cheng, View synthesis-based light field image compression using a generative adversarial network, *Information Sciences* 545 (2021) 118–131.
- [24] D. Liu, L. Wang, L. Li, Z. Xiong, F. Wu, W. Zeng, Pseudo-sequence-based light field image compression, in: *IEEE ICMEW, IEEE*, 2016, pp. 1–4.
- [25] W. Ahmad, R. Olsson, M. Sjöström, Interpreting plenoptic images as multi-view sequences for improved compression, in: *IEEE ICIP, IEEE*, 2017, pp. 4557–4561.

- [26] W. Ahmad, M. Ghafoor, S. A. Tariq, A. Hassan, M. Sjöström, R. Olsson, Computationally efficient light field image compression using a multiview hevc framework, *IEEE access* 7 (2019) 143002–143014.
- [27] J. Gu, B. Guo, J. Wen, High efficiency light field compression via virtual reference and hierarchical mv-hevc, in: *IEEE (ICME)*, IEEE, 2019, pp. 344–349.
- [28] J. Ravishankar, M. Sharma, P. Gopalakrishnan, A flexible coding scheme based on block krylov subspace approximation for light field displays with stacked multiplicative layers, *Sensors* 21 (13) (2021) 4574.
- [29] K. Maruyama, K. Takahashi, T. Fujii, Comparison of layer operations and optimization methods for light field display, *IEEE Access* 8 (2020) 38767–38775.
- [30] M. Le Pendu, C. Guillemot, A. Smolic, A fourier disparity layer representation for light fields, *IEEE TIP* 28 (11) (2019) 5740–5753.
- [31] N. Bakir, W. Hamidouche, O. Déforges, K. Samrouth, M. Khalil, Light field image compression based on convolutional neural networks and linear approximation, in: *2018 25th IEEE International Conference on Image Processing (ICIP)*, IEEE, 2018, pp. 1128–1132.
- [32] Z. Zhao, S. Wang, C. Jia, X. Zhang, S. Ma, J. Yang, Light field image compression based on deep learning, in: *2018 IEEE International Conference on Multimedia and Expo (ICME)*, IEEE, 2018, pp. 1–6.
- [33] B. Wang, Q. Peng, E. Wang, K. Han, W. Xiang, Region-of-interest compression and view synthesis for light field video streaming, *IEEE Access* 7 (2019) 41183–41192.
- [34] C. Jia, X. Zhang, S. Wang, S. Wang, S. Ma, Light field image compression using generative adversarial network-based view synthesis, *IEEE Journal on Emerging and Selected Topics in Circuits and Systems* 9 (1) (2018) 177–189.

- [35] C. Musco, C. Musco, Randomized block krylov methods for stronger and faster approximate singular value decomposition, arXiv preprint arXiv:1504.05477.
- [36] G. J. Sullivan, J.-R. Ohm, W.-J. Han, T. Wiegand, Overview of the high efficiency video coding (hevc) standard, *IEEE TCSVT* 22 (12) (2012) 1649–1668.
- [37] E. Dib, M. Le Pendu, C. Guillemot, Light field compression using fourier disparity layers, in: *IEEE ICIP*, IEEE, 2019, pp. 3751–3755.
- [38] J. Ravishankar, M. Sharma, A hierarchical coding scheme for glasses-free 3d displays based on scalable hybrid layered representation of real-world light fields, *CoRR* abs/2104.09378. arXiv:2104.09378.
URL <https://arxiv.org/abs/2104.09378>
- [39] M. Levoy, P. Hanrahan, Light field rendering, in: *Proceedings of the 23rd annual conference on Computer graphics and interactive techniques*, 1996, pp. 31–42.
- [40] S. J. Gortler, R. Grzeszczuk, R. Szeliski, M. F. Cohen, The lumigraph, in: *Proceedings of the 23rd annual conference on Computer graphics and interactive techniques*, 1996, pp. 43–54.
- [41] W. B. Pennebaker, J. L. Mitchell, *JPEG: Still image data compression standard*, Springer Science & Business Media, 1992.
- [42] G. J. Sullivan, J.-R. Ohm, W.-J. Han, T. Wiegand, Overview of the high efficiency video coding (hevc) standard, *IEEE Transactions on circuits and systems for video technology* 22 (12) (2012) 1649–1668.
- [43] L. Li, Z. Li, B. Li, D. Liu, H. Li, Pseudo-sequence-based 2-d hierarchical coding structure for light-field image compression, *IEEE Journal of Selected Topics in Signal Processing* 11 (7) (2017) 1107–1119.

- [44] T. Senoh, K. Yamamoto, N. Tetsutani, H. Yasuda, Efficient light field image coding with depth estimation and view synthesis, in: 2018 26th European Signal Processing Conference (EUSIPCO), IEEE, 2018, pp. 1840–1844.
- [45] X. Huang, P. An, L. Shan, R. Ma, L. Shen, View synthesis for light field coding using depth estimation, in: 2018 IEEE International Conference on Multimedia and Expo (ICME), IEEE, 2018, pp. 1–6.
- [46] G. Wetzstein, Synthetic light field archive - mit media lab, <https://web.media.mit.edu/~gordonw/SyntheticLightFields/>, accessed: 01-04-2021.
- [47] M. Gu, S. C. Eisenstat, Efficient algorithms for computing a strong rank-revealing qr factorization, *SIAM Journal on Scientific Computing* 17 (4) (1996) 848–869.
- [48] M. Le Pendu, C. Ozcinar, A. Smolic, Hierarchical fourier disparity layer transmission for light field streaming, in: 2020 IEEE International Conference on Image Processing (ICIP), IEEE, 2020, pp. 2606–2610.
- [49] M. Le Pendu, A. Smolic, High resolution light field recovery with fourier disparity layer completion, demosaicing, and super-resolution, in: 2020 IEEE International Conference on Computational Photography (ICCP), IEEE, 2020, pp. 1–12.
- [50] M. Rerabek, T. Ebrahimi, New light field image dataset, in: 8th International Conference on QoMEX, 2016.
- [51] D. G. Dansereau, O. Pizarro, S. B. Williams, Decoding, calibration and rectification for lenselet-based plenoptic cameras, in: Proceedings of the IEEE conference on computer vision and pattern recognition, 2013, pp. 1027–1034.
- [52] G. Bjontegaard, Calculation of average psnr differences between rd-curves, VCEG-M33.

- [53] K. Maruyama, H. Kojima, K. Takahashi, T. Fujii, Implementation of table-top light-field display, in: IDW, 2018.
- [54] Y. Kobayashi, K. Takahashi, T. Fujii, From focal stacks to tensor display: A method for light field visualization without multi-view images, in: IEEE ICASSP, IEEE, 2017, pp. 2007–2011.
- [55] K. Maruyama, Y. Inagaki, K. Takahashi, T. Fujii, H. Nagahara, A 3-d display pipeline from coded-aperture camera to tensor light-field display through cnn, in: IEEE ICIP, IEEE, 2019, pp. 1064–1068.